Available online at www.sciencedirect.com
SCIENCE DIRECT®
International Journal of Heat and Fluid Flow 25 (2004) 351–363
International Journal of HEAT AND FLUID FLOW
www.elsevier.com/locate/ijhff

Low-dimensional analysis, using POD, for two mixing layer–wake interactions

Caroline Braud [a], Dominique Heitz [a], Georges Arroyo [a], Laurent Perret [b], Joël Delville [b,*], Jean-Paul Bonnet [b]

[a] *Cemagref, 17 Avenue de Cucillé, F35044 Rennes Cedex, France*
[b] *Laboratoire d'Etudes Aérodynamiques, UMR CNRS 6609, Université de Poitiers, ENSMA, CEAT, 43, route de l'Aérodrome, F-86036 Poitiers, France*

Abstract

The mixing layer–wake interaction is studied experimentally in the framework of two flow configurations. For the first one, the initial conditions of the mixing layer are modified by using a thick trailing edge, a wake effect is therefore superimposed to the mixing layer from its beginning (blunt trailing edge). In the second flow configuration, a canonical mixing layer is perturbed in its asymptotic region by the wake of a cylinder arranged perpendicular to the plane of the mixing layer. These interactions are analyzed mainly by using two-point velocity correlations and the proper orthogonal decomposition (POD). These two flow configurations differ by the degree of complexity they involve: the former is mainly 2D while the latter is highly 3D. The blunt trailing edge configuration is analyzed by using rakes of hot wire probes. This flow configuration is found to be considerably different when compared to a conventional mixing layer. It appears in particular that the scale of the large structures depends only on the trailing edge thickness and does not grow in its downstream evolution. A criterion, based on POD, is proposed in order to separate wake–mixing layer dominant areas of the downstream evolution of the flow. The complex 3D dynamical behaviour resulting from the interaction between the canonical plane mixing layer and the wake of a cylinder is investigated using data arising from particle image velocimetry measurements. An analysis of the velocity correlations shows different length scales in the regions dominated by wake like structures and shear layer type structures. In order to characterize the particular organization in the plane of symmetry, a POD-Galerkin projection of the Navier–Stokes equations is performed in this plane. This leads to a low-dimensional dynamical system that allows the analysis of the relationship between the dominant frequencies to be performed. A reconstruction of the dominant periodic motion suspected from previous studies is then retrieved.

Keywords: Particle image velocity; Rakes of hot wires; Two-point correlation; Dynamical systems

1. Introduction

Turbulent mixing layers (ML) are dominated by the large scale organization. Canonical mixing layers (CML) have been studied for years. The purpose of this study is to analyze the dynamical behaviour of perturbed ML. ML can be perturbed either from their beginning, by modifying the initial conditions, or further downstream during their development. We consider here both ways by examining two different flow configurations.

For the first case, the initial conditions are modified by imposing a thick trailing edge, a wake effect being superimposed to the ML at the trailing edge (TML). The objective is then to analyze the downstream evolution of the structure of the flow compared to the CML, i.e. a ML emanating from a thin trailing edge. Assuming that the wake effects vanish downstream, it is expected that the TML evolves toward an asymptotic stage. This will be looked into by studying the dynamical behaviour of the flow.

For the second case, the CML is perturbed in its asymptotic region by the wake of a cylinder arranged perpendicular to the plane of the mixing layer (WML).

* Corresponding author. Tel.: +33-5-4936-6057; fax: +33-5-4936-6001.
E-mail address: joel.deville@lea.univ-poitiers.fr (J. Delville).

0142-727X/$ - see front matter © 2004 Published by Elsevier Inc.
doi:10.1016/j.ijheatfluidflow.2004.02.005

In this case also, a wake-type perturbation is imposed to the mixing layer and its effects are examined through a dynamical analysis.

The two cases represent different levels of complexity for a same type of interaction. In the first one, a wake effect is imposed into a mixing layer at the beginning of its development and in the same direction, keeping a 2D global structure in time average. In the second one, a wake is set to develop perpendicularly to a developed mixing layer, leading to a fully 3D interaction.

For both configurations, we shall start with a classical examination of the velocity profiles evolution through the domain, then we shall analyze the dynamics of the flow, focusing on the large scale structures behaviour. For that purpose the proper orthogonal decomposition (POD) is a very powerful technique as it allows the extraction of the energetically dominant modes in the organization of the flow. This decomposition has been widely used in various applications like data compression and mathematical models – see Holmes et al. (1996). Examples for fully inhomogeneous turbulent flows can be found in Manhart (1998) and Alfonsi et al. (2003) who have applied POD behind a mounted cube. Recently POD has been applied to particle image velocimetry (PIV) measurements (Bernero and Fiedler, 2000; Stephen et al., 1999). This data type is strongly limited in time by the actual frame rates of the CCD cameras typically used for PIV. All of POD applications cited above show that it is possible to retrieve the coherent structures observed in experiments. In this paper, we apply the POD to each of the two cases studied, the two sets of data being acquired by means chosen according to the global structure of the flow. For the first case, rakes of hot wire probes are used. The data are then well resolved in time but relatively poorly distributed in space. The second experiment uses the PIV method, from which the spatial definition is high while the temporal statistics remain of lower accuracy. This lower accuracy would correspond, in a Bi-orthogonal Decomposition Approach (BOD: Aubry et al., 1991), to the time delay between each picture, which greatly limits the high-frequency response of the measurement apparatus. However in the classical POD approach developed in the following, this limitation is mainly related to the effective number of pictures that can be reasonably considered, due to storage requirements. However note that in this case, the large time delay between samples due to the PIV limitation can be of advantage because it can be several orders of magnitudes greater than the temporal integral scale. The statistics are then obtained from truly independent statistical events: the statistical convergence can therefore be estimated through the chi-squared rule (see Bendat and Piersol, 1986). Owing to the advantages and limitations of the two experimental methods the analysis tools will be slightly different but in both cases a spatio-temporal analysis will be carried on, based on correlations and on the POD treatment.

The POD can be used as a tool for physical interpretation, but also can be used in truncated form to produce a low-order dynamical model of the flow (LOD). Ruelle and Takens (1971) proved with a theoretical approach that a few degrees of freedom is enough to get a chaotic dynamic system. Holmes et al. (1997) showed that an attractor representation in the phase space exists if there is an exponential decay of the empirical eigenvalues extracted from POD analysis. Hence, most of the POD studies are followed by a Galerkin projection, which is a projection of the Navier–Stokes equation onto the orthogonal basis of the POD (Aubry et al., 1988; Ukeiley et al., 2001; Ma and Karniadakis, 2002). In this way, a partial differential equation is reduced to an ordinary differential equation which can be analyzed with stability theory. This approach will be followed for the second experiment.

2. Turbulent mixing layer downstream a thick trailing edge: TML

Several authors have shown that the development of turbulent mixing layers is very sensitive to the inflow conditions. Parameters such as the momentum thickness of the boundary layers at the trailing edge or their laminar or turbulent state have a strong influence on the downstream behaviour of the flow, especially on the growth rate of the mixing layer and on the location of the self-similar region. In particular, Dziomba and Fiedler (1985) showed experimentally the importance of the trailing edge thickness h. They found that if this parameter exceeds 50% of the sum of the boundary layer displacement thicknesses δ_1 on the splitter plate, its influence becomes significant and modifies both the spreading rate and the characteristic frequencies of the flow, the instability frequency of the wake becoming dominant. They also confirmed the theoretical demonstration by Michalke and Schade (1963) of the strong influence of the wake component of the longitudinal velocity profiles on the Strouhal number. In his study of the plane mixing layer development, Metha (1991) found that the splitter plate wake and its complex interaction with the mixing layer play a dominant role, especially in the way the self-similar state is reached. Koch (1985) investigated self-excited wake flow development (more particularly flows past a blunt edged flat plate) by means of stability analysis. He showed that the nature of the flow instability, which can be either convective or absolute, is directly related to the asymmetry of the initial conditions, namely the external velocity ratio and the difference in the characteristics of the boundary layers on the splitter plate.

Quantities such as the spreading rate or the characteristic frequency, which depend on the inflow conditions, are characteristic of the large scale structures of the flow. As a consequence, techniques such as conditional and structural averaging (Antonia, 1981) or Proper Orthogonal Decomposition (POD) introduced by Lumley (1967) can be used to study the influence of the trailing edge geometry on the downstream development of the flow. George and coworkers have shown that the initial conditions can strongly influence the self-similar characteristics. They tend to relate this influence to the large scale structures through POD analysis (Johansson, 2002; Johansson et al., 2002).

In the present work, we analyze the influence of the wake effect of the splitter plate trailing edge on the downstream evolution of a turbulent mixing layer. In this case the ratio between the trailing edge thickness and the displacement thickness of the boundary-layers h/δ_1 is about 10. This kind of flow is of interest because it is expected to exhibit different behaviours, presenting simultaneously two types of global instability. An absolute instability due to the splitter plate wake influence and a convective instability, characteristic of the mixing layer behaviour can be found simultaneously in such a flow (Koch, 1985).

2.1. Experimental set-up

The experiments were carried out in an 0.3×0.3 m^2 open wind-tunnel. The two-dimensional subsonic turbulent mixing layer had a high speed velocity U_a of 35.2 m/s and a low speed velocity U_b equal to 23.8 m/s (velocity ratio $r = 0.67$). The two mixing flows merging at the trailing edge were turbulent with typical momentum thicknesses of 0.85 mm. The thickness of the trailing edge h was equal to 19 mm. The Reynolds number based on ΔU the difference of velocity between the two flows and h was $Re = h\Delta U/\nu \simeq 14,400$. In order to be able to quantify the wake effect, the splitter plate trailing edge can be either bevelled (canonical mixing layer (CML)) or blunt (configuration named here thick mixing layer (TML)). The half-angle of the bevel (12°) was chosen to avoid any flow separation in this region.

The measurements were systematically performed in both configurations at different downstream locations (from $x/h = 5.25$ to $x/h = 42.1$) by using hot wire anemometry. A rake of 19 non-uniformly spaced X-wires probes was used to obtain both the longitudinal and the transversal (normal to the plate) velocity components. The probes were placed symmetrically about the mixing layer axis with a separation of 4.0 mm near the centre of the shear layer and 8.0 mm in the external region, the rake spanning 93 mm ($4.9h$).

2.2. Flow visualisations

Flow visualisations were performed by injecting smoke into the flow at the trailing edge of the splitter plate. From instantaneous photographs (Fig. 1), the thick mixing layer clearly exhibits a strong organization and larger scales when compared to the CML. More particularly, two rows of opposite sign vortices located at the top and the bottom edges of the trailing edge of the splitter plate can be observed in Fig. 1(a). The top and bottom vortices are not strictly alternating like in a classical wake but seem to be almost vertically aligned with the low speed structures being captured by the high speed ones. Hence they tend to merge downstream to form only one row. That results in a large increase of the growth rate of the shear layer.

2.3. Mean velocity profiles

The mean longitudinal velocity profiles (Fig. 2) measured at different streamwise locations show the strong influence of the wake effect when a blunt trailing edge is used. A velocity defect can be observed up to $x/h \simeq 52$. As a consequence, the self-similarity region is reached very far downstream. Moreover, it is noticeable that the thick mixing layer develops essentially on the high velocity side of the flow. In both their experimental and numerical studies of the vortex shedding from a blunt trailing edge with unequal external mean velocities, Boldman et al. (1976) found also such behaviour when the mean velocity ratio is below 1. The growth rate of the mixing layer vorticity thickness $\delta_\omega = \Delta U/(\mathrm{d}\bar{u}/\mathrm{d}y)_{\max}$ confirms the high expansion rate of the thick

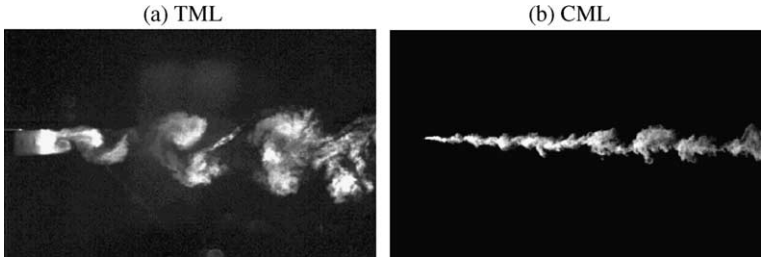

Fig. 1. Instantaneous flow vizualisations for the TML and CML cases (same scale: nearly 13.7 $x/h \times 8.4$ x/h).

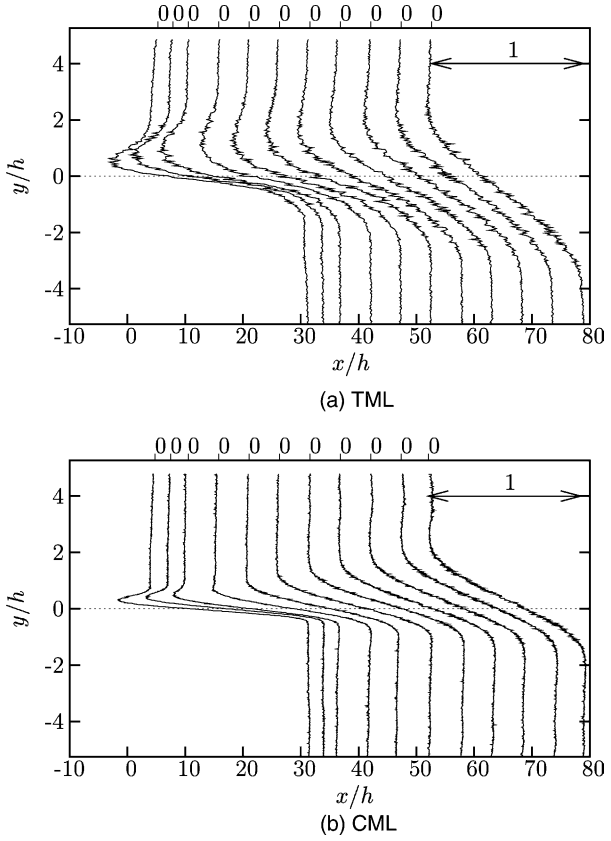

Fig. 2. Mean longitudinal velocity profiles for the TML and CML cases.

mixing layer at about twice the rate of the conventional mixing layer (respectively, $d\delta_\omega/dx = 0.0684$ and 0.0371).

2.4. Longitudinal evolution of the Reynolds shear stress

The Reynolds shear stress profiles obtained with a blunt trailing edge are plotted as a function of the streamwise distance in Fig. 3. Consistently with the mean velocity profiles, they exhibit two different behaviours revealing the different regions involved in this flow:

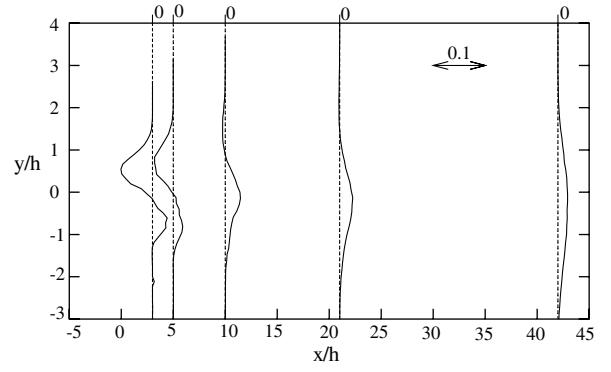

Fig. 3. Streamwise evolution of the Reynolds shear stress $\overline{u'v'}/\Delta U^2$ in the TML case.

- In the near wake ($x/h < 16$), two peaks of opposite signs can be observed. The high-speed side has a positive peak whereas the other side has a negative extremum decreasing with the downstream distance and eventually disappearing. It is worth noting that the negative peak is more important in magnitude than the positive one in the near region.
- For x/h greater than typically 16, the effect of the wake disappears and is overcome by the mixing layer influence. The Reynolds stress profiles have the classical shape found for a conventional mixing layer with only one positive extremum.

Metha (1991) found the same type of behaviour in his study of the effect of the velocity ratio on the plane mixing layer development, showing that the magnitude of the low-speed side Reynolds stress peak is an increasing function of the velocity ratio. For all the velocity ratios Metha (1991) explored, the high-speed side extremum was found to be always greater than the second peak which is contrary to our results. This difference can be attributed to the fact that Metha used a thinner trailing edge with regard to δ_1 reducing the strength of the wake effect.

2.5. Space–time correlations

Space–time correlation coefficients were obtained with the rake of X hot wires and were computed for each velocity component as follows:

$$C_{ii}(y, y', \tau) = \frac{\langle u_i(y,t) u_i(y', t+\tau)\rangle}{\sqrt{\langle u_i(y,t)^2\rangle}\sqrt{\langle u_i(y',t)^2\rangle}}$$

where $\langle\cdot\rangle$ is the conventional time average, here equivalent to an ensemble average while dealing with steady flow configurations (stationary and ergodic statistical properties). For the sake of simplicity, we focus in the present paper on the longitudinal u-component of the velocity ($i = 1$). These statistics permit us to characterize the spatio-temporal organization of the flow. Fig. 4 shows a typical example of these correlations at $x/h = 5.25$ for the CML and TML flow configurations. The reference probe was located at $y/h = -0.84$. The u-component correlations show alternating positive and negative correlated areas both in the temporal and the transverse directions. The thick mixing layer appears to be strongly correlated in time whereas the correlation levels decrease rapidly in the conventional case. The v-component (not presented here) has the same temporal behaviour but its sign does not change with respect to the y-direction.

The experiments performed at other downstream locations (see Fig. 4 for the correlations of the u-component at $x/h = 21$) show the same type of time-correlation and a similar downstream organization. In the

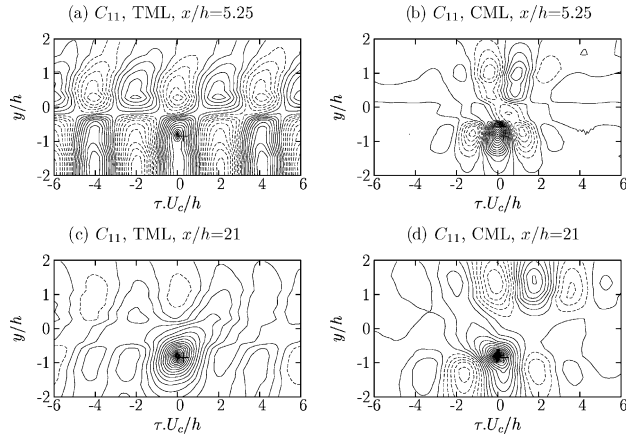

Fig. 4. Spatio-temporal correlation of the longitudinal velocity component measured at two streamwise locations: (—) positive correlations; (- - -) negative correlations. Reference probe located at $y/h = -0.84$.

case of the blunt trailing edge, the temporal wavelength of the alternate areas appears to be constant with the streamwise direction with a typical time scale $\tau_0 U_c/h = 4$. Although the correlation levels being less important than upstream, τ_0 remains constant for both x values. On the contrary, for the conventional mixing layer, it evolves linearly: the further downstream, the greater the wavelength is. These results confirm that the mixing layer past the blunt trailing edge is dominated by the wake effect for a long time and the large scales of the flow seem to be governed by the trailing edge thickness. The wake effect is to force the flow in time, the large structures being locked on a specific scale. In the case of the bevelled trailing edge mixing layer, the large scale organization is scaled to the local vorticity thickness, then evolves linearly with the downstream location.

2.6. Application of POD

In this section, the proper orthogonal decomposition is briefly presented. More details can be found in Berkooz et al. (1993). Lumley (1967) first proposed the POD technique to identify the coherent structures in turbulent flows. It consists of extracting from the flow the structure $\mathbf{\Phi}(\mathbf{X})$ which maximises the projection of the velocity-field $\mathbf{u}(\mathbf{X},\mathbf{t})$ in a mean-square sense.

This maximization problem leads to solve the integral problem of eigenvalues:

$$\int_{\mathscr{D}} R_{ij}(\mathbf{X},\mathbf{X}')\phi_j^{(n)}(\mathbf{X}')\,\mathrm{d}\mathbf{X}' = \lambda_n \phi_i^{(n)}(\mathbf{X}) \tag{1}$$

where R_{ij} is the spatial space correlation tensor over the domain $\mathscr{D}$:

$$R_{ij}(\mathbf{X},\mathbf{X}') = \langle u_i(\mathbf{X}) u_j(\mathbf{X}')\rangle \tag{2}$$

The fluctuating field can be projected onto the POD basis composed of the n eigenfunctions $\phi_i^{(n)}(\mathbf{X})$:

$$u_i(\mathbf{X},t) = \sum_{n=1}^{\infty} a^{(n)}(t)\phi_i^{(n)}(\mathbf{X}) \tag{3}$$

Two kinds of eigenvalues problems can be solved, depending on the kernel which is used. A *spatial POD* can be performed if the POD kernel is the two-point spatial correlation tensor $R_{ij}(\mathbf{X},\mathbf{X}') = \langle u_i(\mathbf{X})u_j(\mathbf{X}')\rangle$. If the kernel is the cross-spectrum spatial correlation tensor $S_{ij} = (\mathbf{X},\mathbf{X}';f) = \langle \tilde{u}_i(\mathbf{X};f)\tilde{u}_j^*(\mathbf{X}';f)\rangle$ where $\tilde{g}$ is the Fourier transform of g and $\tilde{g}^*$ is the complex conjugate of $\tilde{g}$, a *spectral POD* is computed. Practically we solve this problem by considering the following matrix diagonalization problem,

$$\mathbf{A\Phi} = \mathbf{\Lambda\Phi} \tag{4}$$

and by finding the eigenvectors and eigenvalues of a symmetrical definite-positive matrix $\mathbf{A}$ which is a discrete representation of the two point velocity cross-correlation tensor.

Note that in the present section, only the transversal direction (i.e. $\mathbf{X} = y$) is considered for the decomposition.

2.7. Spatial POD results

In this section, a scalar POD approach is used: each velocity component is computed independently using the two-point spatial correlation tensor $R_{ii}(y,y') = \langle u_i(y)u_i(y')\rangle$ ($i = 1$ or 2).

Fig. 5 shows the first two POD modes of the longitudinal velocity component obtained at different downstream locations for the two mixing layer configurations.

In the case of the bevelled trailing edge, the classic behaviour of the first two modes is retrieved (see Delville, 1999): the shape of the first mode is approximately a Gaussian centred on the mixing layer axis, and the second mode is antisymmetric.

As regards to the thick mixing layer, the shapes of the first two modes depend on the longitudinal position considered:

- When the longitudinal distance from the trailing edge is greater than typically $16h$, the shapes of the first two modes are similar to the conventional case CML.
- For $x/h \in [0 : 15.8]$, the first mode is almost antisymmetric whereas the second one looks more Gaussian in form. Thus, in the near region, the POD modes of the thick mixing layer behave like those of a flat plate wake (Delville, 1995).

This change of the shape of the first two modes with the longitudinal distance is quite similar to that of the Reynolds stress $\overline{u'v'}$ and can be interpreted as the influence of the wake effect on the shear layer. Considering the behaviour of the u-component POD modes, the near region is dominated by the wake mode of the

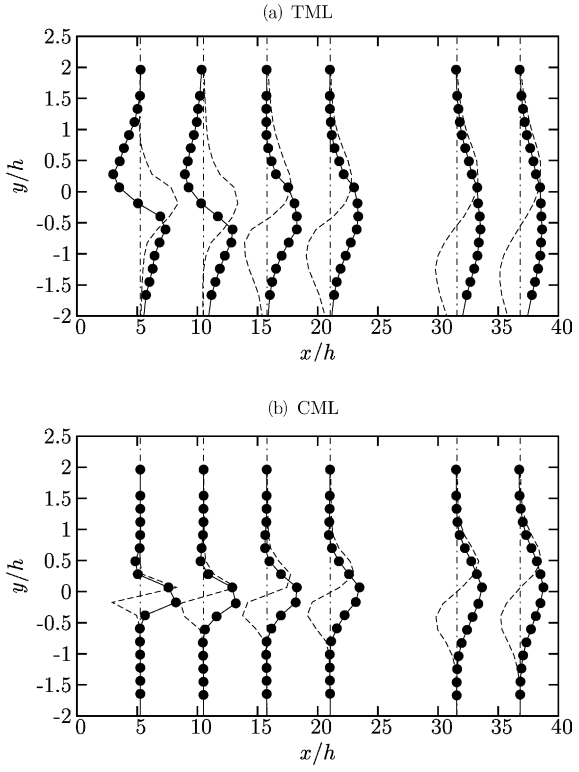

Fig. 5. Streamwise evolution of the first two POD modes of the longitudinal velocity component: (a) TML; (b) CML. Plotted are: (–●–) $\phi^{(1)}(y)$; (- - -) $\phi^{(2)}(y)$ (arbitrary scale).

flow, whereas further downstream, the shear layer tends to behave like a conventional mixing layer. It appears that *only the first two POD modes are modified* by the wake influence. The higher order modes of the two kinds of flow have the same shape. The interpretation can be that only the large structures of the flow were strongly altered by the wake of the plate.

Fig. 6 shows the longitudinal evolution of the relative importance of the first and the second mode (λ_1/λ_2). The ratio of the first two eigenvalues first decreases with the distance from the trailing edge, reaching a minimum of 1.2 at $x/h = 15.8$ and then increases. The upstream region is clearly dominated by the first mode which is

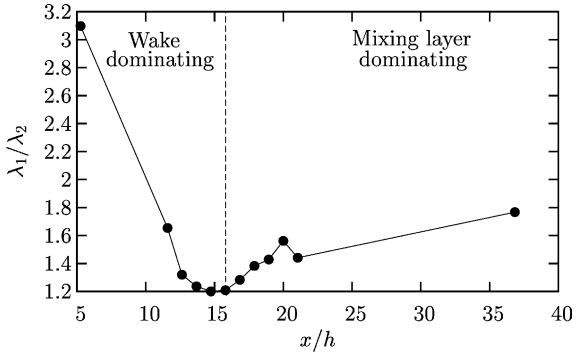

Fig. 6. Streamwise evolution of the ratio λ_1/λ_2 in the TML case.

there antisymmetric whereas for $x/h > 15.8$, the most energetic mode is symmetric. It should be pointed out that there exists a *transition* region ($x/h \simeq 15.8$) in which the shape of the first two modes change and their corresponding eigenvalues are of the same order of magnitude. Thus, the behaviour of the ratio of the first two eigenvalues reveals where the important modification of the flow organization occurs.

2.8. Spectral POD results

The strong influence of the wake in the near region ($x < 15.8$) is also found when a *spectral* POD is computed.

The computation of the POD modes of u confirms the change of the shape of the first two modes. Fig. 7 presents the modulus of the first mode weighted by the root of the corresponding eigenvalue. At $x/h = 5.25$ (Fig. 7(a)), the first mode presents two peaks for $f = 380$ Hz located on each side of the shear layer whereas downstream ($x/h = 36.8$, Fig. 7(c)) only one maximum at lower frequencies located on the mixing layer axis can be observed.

Nevertheless, the frequency dependence of the POD modes shows that the transition from a wake dominated

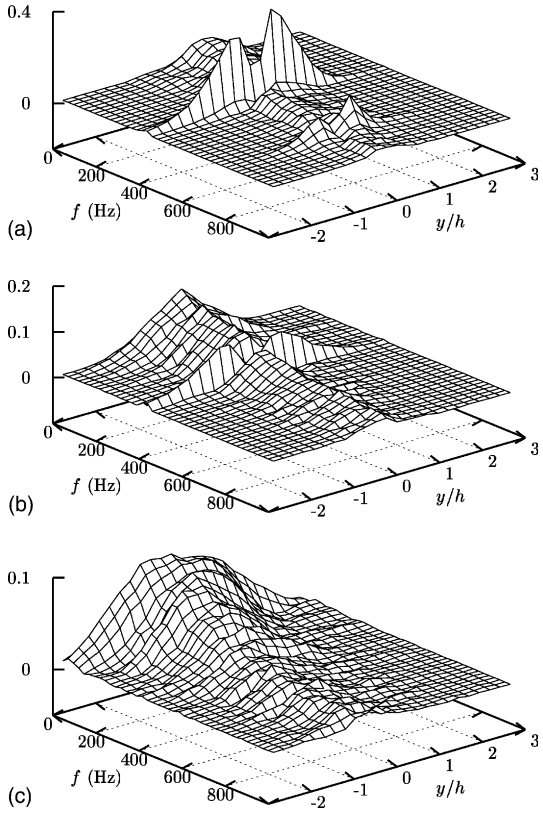

Fig. 7. Evolution of the first mode ($\sqrt{\lambda_1}\phi^{(1)}$) of the longitudinal velocity component obtained by spectral POD in the TML case: (a) $x/h = 5.25$; (b) $x/h = 21$; (c) $x/h = 36$ (arbitrary but everywhere the same scale).

flow to a more conventional mixing layer is more progressive than expected from the spatial POD mode results. At $x/h = 21$, the first spectral POD mode (see Fig. 7(b)) exhibits two peaks at the frequency characteristic of the wake Strouhal number ($f = 380$ Hz) but also a maximum at a lower frequency located on the mixing layer axis (like the first mode at $x/h = 36.8$). However the peak of the 380 Hz mode in Fig. 7(b) is lower than in Fig. 7(a) and the total energy in the 380 Hz mode is small compared with the total energy in Fig. 7(b), that is why the effect of the wake is not seen in the spatial POD results. At $x/h = 36.8$ the shape of the first spatial POD mode is already Gaussian, as observed in the bevelled trailing edge mixing layer.

3. Turbulent mixing layer interacting with a cylinder wake: WML

In the second configuration, the wake is imposed across the mixing layer further downstream in the asymptotic region. That type of interaction between a plane mixing layer and the wake of a slender body is of great interest as it occurs in practical environmental and industrial configurations.

Previous studies of this flow showed that strong interactions take place just behind the shedding body (Heitz, 1999). In the near wake, a non-stationary secondary flow from the low to the high velocity side of the shear layer was observed in video sequences. Some classical phenomena were also highlighted, like the presence of cells of constant shedding frequency under the action of a velocity shear in the spanwise direction of the cylinder. From spectral analysis, it was found that some complex three-dimensional organization was taking place in the mixing layer–wake interaction region. These findings suggested that the understanding of the peculiarities of that flow demands a description of the three-dimensional dynamics of the coherent structures of the flow.

3.1. Experimental set-up

Experiments were performed in a 0.3×0.3 m^2 closed-loop wind tunnel (for more details see Heitz, 1999). The velocity ratio between the two streams was $r = U_b/U_a = 0.65$, with an average convective velocity $U_m = (U_a + U_b)/2 = 14.85$ m/s ($U_a = 18$ and $U_b = 11.7$ m/s) giving an average Reynolds number, based at the cylinder diameter $D = 8$ mm, of 7920. Preliminary hot-wire measurements have shown that without the cylinder, the plane mixing layer reaches the turbulent self-similarity state at a downstream distance of 140 mm from the trailing edge of the splitter plate. The expansion factor $\sigma = \sqrt{\pi}(\mathrm{d}\delta_\omega/\mathrm{d}x)^{-1}$ is found to be about 48. The circular cylinder is placed at 160 mm from the origin of the mixing layer, so that its diameter corresponds to the local vorticity thickness at the cylinder location, $\delta_{\omega_0} = D = 8$ mm. The coordinate system is x in streamwise direction, y in cross-stream (vertical, parallel to the axis of the cylinder) and z in spanwise direction (parallel to the plate). The origin is taken so that $x = 0$ and $z = 0$ on the cylinder axis and $y = 0$ on the centreline of the trailing edge of the splitter plate (Fig. 8). The $z = 0$ plane represents the plane of symmetry that will be used for the development of the dynamical system. In this last development we will focus on the analysis of a subset of a more complex experiment where the correlation tensor involving the two velocity components (u and v) was measured by using PIV over a three-dimensional domain (see Braud et al., 2002). We focus here on the (x–y) planes for which the measurement domain is $L_x \times L_y = 10.5 \times 7.75D^2$. This area is limited to the near downstream zone of the cylinder.

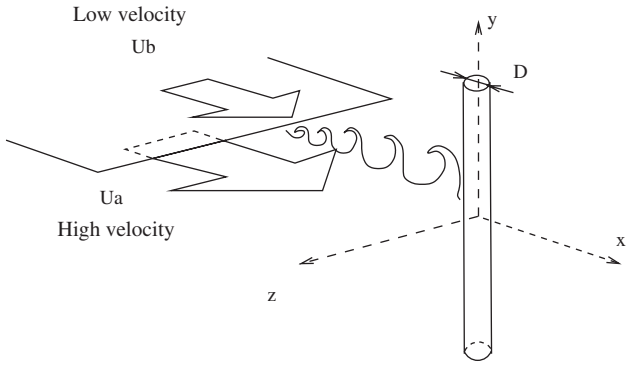

Fig. 8. Schematic view of the WML flow configuration.

3.2. Mean velocity profiles

The main topological characteristics found from this PIV experiment are very close to that found in previous results by other experimental means (Heitz, 1999). The global behaviour of this particular flow can be observed from the mean velocity profiles, plotted in Fig. 9 in a z–y plane at $x = x_a = 5.53D$ (near the centre of the domain in the x-direction). From the streamwise mean velocity profiles U, one can observe the footprint of the mixing layer and that of the wake for $|z/D| \sim 4$ and for $|y/D| \sim 3$, respectively, while for smaller values of z and y, the wake–mixing layer interaction zone shows that the velocity deficit corresponding to the high velocity side is of the order of magnitude of ΔU (Fig. 9(a)). In this region, a strong global flow motion towards the high velocity side can be observed. For $|z/D| < 1$, the vertical velocity mean component $\bar{v}$ is of the order of $0.2\Delta U$, on the high velocity side (Fig. 9(b)). This strong motion is even more important closer to the cylinder, where $\bar{v}$ tends to be of the same order of magnitude as ΔU, as

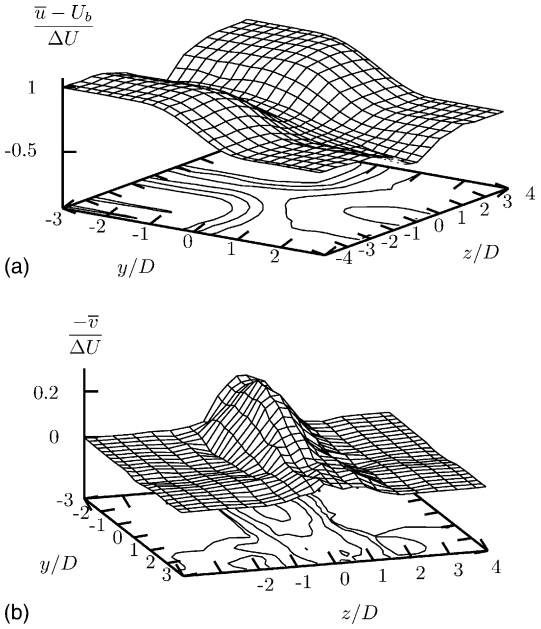

Fig. 9. Mean velocity components in the streamwise plane ($x = 5.53D$): (a) $\frac{\overline{u}-U_b}{\Delta U}$; (b) $\frac{-\overline{v}}{\Delta U}$ WML configuration.

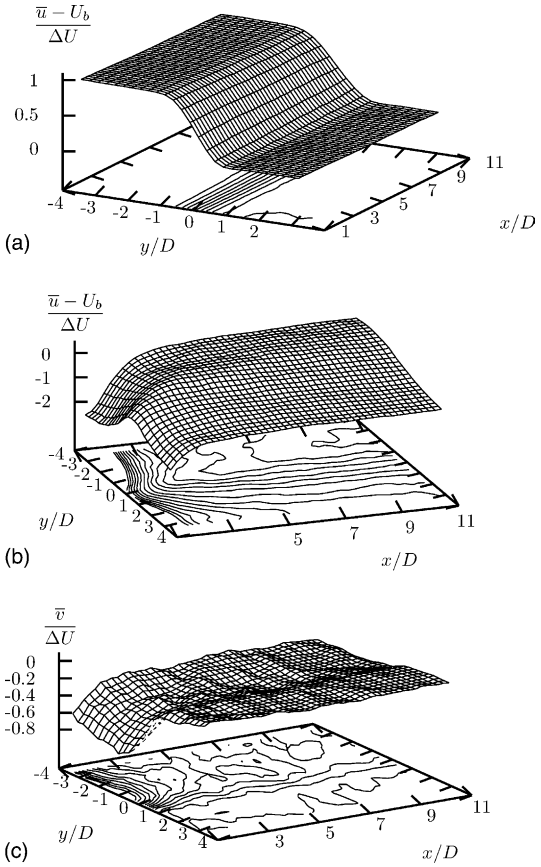

Fig. 10. Mean velocities: (a) spanwise plane ($z = -4D$) $\frac{\overline{u}-U_b}{\Delta U}$; plane of symmetry ($z/D = 0$); (b) $\frac{\overline{u}-U_b}{\Delta U}$; (c) $\frac{\overline{v}}{\Delta U}$. WML configuration.

can be seen in Fig. 10(c) for low x values, in the wake central plane $z = 0$.

The streamwise evolution of the mean flow is illustrated in Fig. 10 where velocities are plotted in x–y planes. In the plane far from the cylinder influence, $z/D = -4$ (Fig. 10(a)), the mean streamwise velocity $\bar{u}$ profiles exhibit a typical mixing layer evolution, with a linear growth and an expansion factor of $\sigma = 47.8$ close to that found in the mixing layer without the circular cylinder ($\sigma = 48$). In the symmetry plane $z/D = 0$ the length of the recirculation zone behind the cylinder (x distance with negative value of $\bar{u}$) can be estimated on the $\bar{u}$ profiles for each value of y (Fig. 10(b)). This length is greater on the high velocity side than on the low velocity side, with a contraction in the mixing layer, near $y/D = 0$. This unusual relation between the incident velocity on the cylinder and the length of the vortex formation zone is clearly specific of the influence of the mixing layer on the wake. This behaviour, previously highlighted by Heitz (1999) and Lamballais and Silvestrini (2002), is in complete opposition with what the literature gives for the evolution of the length of the vortex formation zone for the same values of the local Reynolds number. Here this length is increased (instead of reduced) on the high velocity side of the mixing layer, this phenomenon being probably related to the secondary flow observed from the low to the high velocity side in the very near region of the wake.

3.3. Two point correlations

The first step in the analysis of the organization of this flow configuration involves the examination of the velocity correlations. Fig. 11 shows such correlations obtained for the streamwise fluctuating velocity component, u, in various x–y planes, with $z = z'$. Correlations are shown for the planes that correspond to the *mixing layer like behaviour* zone ($z/D = 4$) (a), the wake–shear area ($z/D \sim 0.9$) (b) and the cylinder axis ($z/D = 0$) (c). In these plots, the reference point (x_a, y_a) is located at the centre of the investigation domain. This position corresponds to the intersection of the drawn horizontal and vertical lines, $x/D = 5.9$, $y/D = 0$. For each plot in Fig. 11 a set of 10 iso-contours are shown for the positive and negative correlation values. They are equally distributed between the minimum negative and maximum positive level, respectively. As can be observed in this figure, the correlations change greatly in shape and integral length scales, depending on the spanwise location of the x–y plane. Integral streamwise length scales Λ_x can be extracted from these plots, provided by the distance between the centres of the negative iso-contours zones surrounding the positive correlation area near the reference point. These scales can be related to conventional Strouhal numbers, through a Taylor hypothesis: $S_t = f_p \mathscr{L}/U_m = \mathscr{L}/\Lambda_x$ where f_p is the typical *structure*

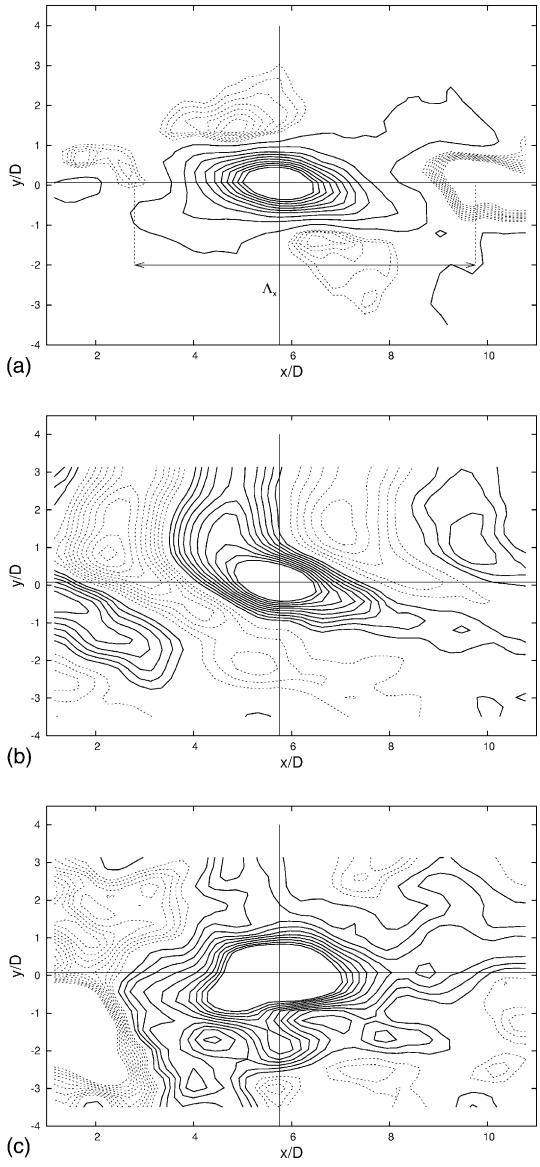

Fig. 11. Iso-contours of correlation $\overline{u(x_a,y_a)u(x,y)}$ in the WML: (–) positive level; (...) negative level; (a) $z/D=-4$; (b) $z/D=-0.87$; (c) $z/D=0$.

passing frequency and $\mathscr{L}$ is a *local size of the structures* e.g. the vorticity thickness δ_ω. In the mixing layer flow, $z/D=-4$, Fig. 11(a), using $\delta_{\omega_a}\simeq 11.5$ mm at $x=x_a$, S_t is found to be 0.22 what is in good agreement with its conventional value measured on a mixing layer axis (Delville et al., 1999). An equivalent passing frequency can then be defined $f_{p_a}\sim 300$ Hz.

In the wake–shear area ($z/D=-0.9$), the streamwise correlations exhibit a high level of spatial organization (Fig. 11(b)). This organization is different for each side of the mixing layer axis. On the high velocity side, a strong slant appears in the correlation function, which begins at the splitter plate level, $y/D=0$. The Strouhal number, $S_t=0.22$, on the high speed side is close to that found in the mixing layer region.

This result confirms the organization pattern discussed in Braud et al. (2002). It has been related to the mixing layer, which gives rise to the simultaneous presence of two types of cell arrangement, with two different frequencies. This results in the propagation of an oblique shedding mode on both sides of the wake, i.e. the high velocity and low velocity side of the wake. Furthermore, this oblique shedding is associated with a contraction of the length of the formation zone at $y/D=0$, Fig. 10(b). In the plane of symmetry, $z/D=0$, the correlations show a particular organization with an integral length scale ($\Lambda_x\sim 12D$) which is twice that found in the mixing layer area, Fig. 11(c). This length scale can be associated to a frequency of the order of $f\simeq 150$ Hz. This observation, associated with a global movement toward the high velocity side, found from the mean velocity-field, highlights the peculiar organization of the flow in this plane.

In order to develop a better understanding of this specific organization, a low-order dynamical system (LODS) approach is implemented, in this plane via a POD-Galerkin projection.

3.4. POD eigenvectors

In order to extract the POD eigenvectors from the symmetry plane, $z/D=0$, a slice POD was applied, where only correlations in this plane were taken into account. The formalism introduced in the previous section is followed. However, unlike the application devoted to the TML, in this part of the work, no temporal evolution could be obtained because PIV low frequency data acquisition was used to built the necessary statistics.

The correlation tensor is obtained here from block ensemble average, according to stationary and ergodicity hypothesis, $R_{ij}(\mathbf{X},\mathbf{X}')$ where $\mathbf{X}=(x,y)$. The size of the discrete correlation tensor, $\mathbf{A}$ to be solved (Eq. (4)) is equal for 2 velocity components to $N=45\times 27\times 2=2430$ which is the number of discrete eigenvalues to be calculated.

In this decomposition, 12% of the total number of modes are enough to retrieve 99% of the total energy. Due to the huge size of the POD problem solved 12% still correspond to 269 modes. As a compromise between the need to reduce the size of the system to be solved and the concern for keeping a significant part of total energy, we retained the 15 first modes which contained 43.5% of the total energy for the POD-Galerkin projection.

Corresponding eigenvectors were calculated. The first and second POD modes, shown in Fig. 12(a) and (b), exhibit movement of large scales from the high velocity side to the low velocity side of the shear layer. For higher modes, above mode 4, smaller scales appear to be superimposed on the large scales. As an example the mode 15 is shown in Fig. 12(c).

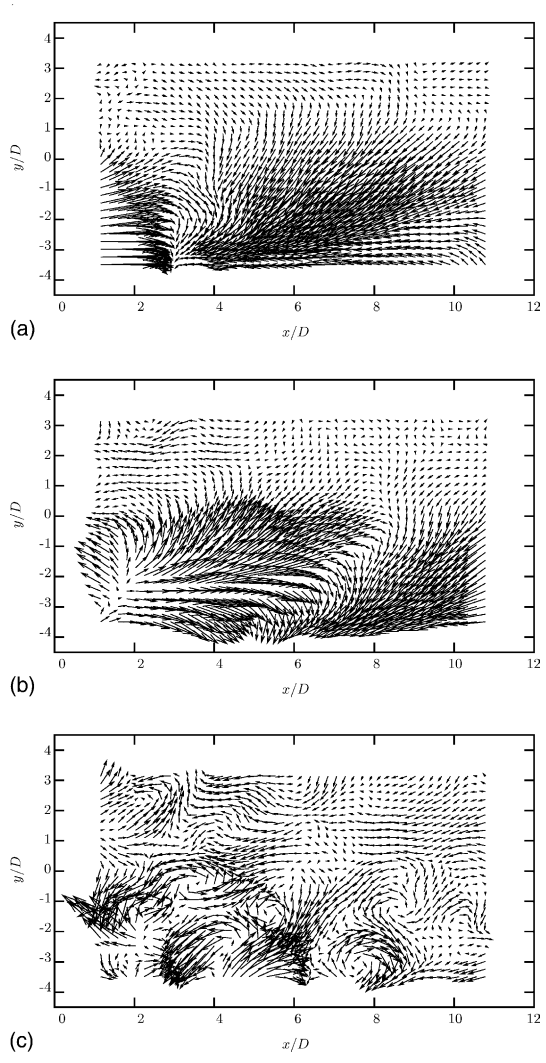

Fig. 12. Eigenvector fields from a 2D2C POD in the WML at $z/D = 0$: (a) mode 1; (b) mode 2; (c) mode 15.

3.5. POD-Galerkin

The first N_{gal} modes being retained, a Galerkin projection of the fluctuating vorticity formulation of the Navier–Stokes equations was performed to develop a LODS. This formulation is preferred here, because it causes the explicit pressure contribution to vanish.

Considering a tridimensional, three components approach, the fluctuating velocity-field $\mathbf{u}$ is expressed as a linear combination of the POD modes (3), and the decomposition of the fluctuating vorticity field $\boldsymbol{\Omega}$ is expressed as

$$\Omega_i(\mathbf{X}, t) = \sum_{n=1}^{N_{\text{gal}}} a^{(n)}(t)\Psi_i^{(n)}(\mathbf{X}) \tag{5}$$

where $\boldsymbol{\Psi}^{(n)}(\mathbf{X}) = \text{rot}(\boldsymbol{\Phi}^{(n)}(\mathbf{X}))$. Note that the 'modes' Ψ, while being a basis of the flow, are not orthonormal. The Galerkin projection of the fluctuating vorticity formulation of the Navier–Stokes equations gives

$$\sum_{n=1}^{N_{\text{gal}}} \int_{\mathscr{D}} \boldsymbol{\Psi}^{(n)} \left(\frac{\partial \boldsymbol{\Omega}}{\partial t} + \mathbf{u} \cdot \nabla \boldsymbol{\Omega} - \boldsymbol{\Omega} \cdot \nabla u + \frac{1}{Re} \nabla^2 \boldsymbol{\Omega} \right) \mathrm{d}\mathbf{X} = 0 \tag{6}$$

This projection leads to the following set of equations, for $n = 1$, N_{gal}, where N_{gal} is the number of modes included in the reconstruction and where time dependency of the a's has been suppressed for the sake of readability

$$\sum_{m=1}^{N_{\text{gal}}} \alpha_{nm} \frac{\mathrm{d}a^{(m)}}{\mathrm{d}t} = \sum_{m=1}^{N_{\text{gal}}} \beta_{nm} a^{(m)} + \sum_{m=1}^{N_{\text{gal}}} \sum_{k=1}^{N_{\text{gal}}} \gamma_{nmk} \left(a^{(m)} a^{(k)} - \langle a^{(m)} a^{(k)} \rangle \right) \tag{7}$$

The coefficients α_{nm} appearing in (7) are a direct consequence of the non-orthonormality of the $\boldsymbol{\Psi}^{(n)}$. Details about coefficients α_{nm}, β_{nm} and γ_{nmk} can be found in Appendix A. In matrix formulation, if the matrix $[\alpha_{nm}]$ is invertible, Eq. (7) can be written, in a conventional ODE approach, through matrix multiplication of its lhs and rhs by $[\alpha_{nm}]^{-1}$, leading to the conventional ODE formulation:

$$\frac{\mathrm{d}a^{(n)}}{\mathrm{d}t} = \sum_{m=1}^{N_{\text{gal}}} \left[\boldsymbol{L}_{nm} + \frac{1}{Re}(1+\alpha)\mathbf{L}'_{nm} \right] a^{(m)} + \sum_{m,k=1}^{n_{\text{gal}}} \boldsymbol{Q}_{nmk} \left(a^{(m)} a^{(k)} - \langle a^{(m)} a^{(k)} \rangle \right) \tag{8}$$

where $\boldsymbol{L}$ corresponds to the mean flow-fluctuating field interaction, $\boldsymbol{L}'$ corresponds to contributions from the viscous effects and $\boldsymbol{Q}$ corresponds to the non-linear velocity contributions. The coefficient $\boldsymbol{\alpha}$ is added in such a way that neglected higher POD modes contribution to the system can be taken into account, by adding some 'artificial' dissipation to the system. Details about coefficients $\boldsymbol{L}$, $\boldsymbol{L}'$ and $\boldsymbol{Q}$ can be found in Appendix A.

In this study, the 3D equations were considered in the plane of symmetry, $z/D = 0$. A spanwise contribution was added as given by the continuity equation, [1] $\Phi_{w,z} = -\Phi_{u,x} - \Phi_{v,y}$ and $\bar{w}_{,z} = -\bar{u}_{,x} - \bar{v}_{,y}$. We note that this formulation is equivalent to considering odd (Φ_w) and even (Φ_u, Φ_v) eigenvector components with respect to the plane of symmetry. To model the contribution of Φ_{v,x,z^2} and Φ_{u,y,z^2} we used an assumption of local isotropy,

$$\Phi_{v,x,z^2} = 2\Phi_{v,x,y^2} \quad \text{and} \quad \Phi_{u,y,z^2} = 2\Phi_{v,y,x^2} \tag{9}$$

The mean velocity profile from experiments was used to calculate coefficients in Eq. (8). To model mean velocity-fluctuation interaction $\langle a^{(m)} a^{(k)} \rangle$, we assumed that the coefficients $a(t)$ satisfy the POD decomposition and hence $\langle a^{(m)} a^{(k)} \rangle = \lambda^{(m)} \delta_{mk}$. Explicit expressions for

[1] We note $f_{u,x} = \frac{\partial f_u}{\partial x}$, $f_{u,x,z^2} = \frac{\partial^3 f_u}{\partial x \partial z^2}$.

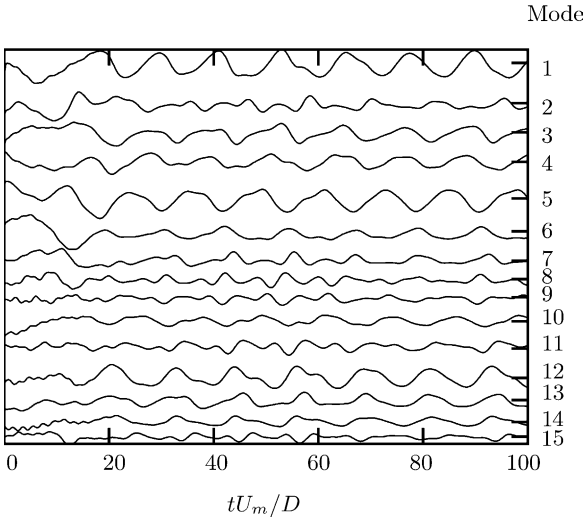

Fig. 13. Time evolution of $a^{(n)}(t)$ from the 15 equations dynamical system, $\alpha \sim 20$ (arbitrary scale).

the coefficient matrices $\boldsymbol{L}$, $\boldsymbol{L}'$ and $\boldsymbol{Q}$ can be found in Appendix A ((A.5)–(A.8)).

Eq. (8) was solved using a Fourth order Runge–Kutta integration. Several tests were conducted on the variation of the number α. The retained level of truncation, 15 equations from the original 2430, leads to a great loss of dissipation and a trivial solution is found for $\alpha = 30$. Below a critical level of $\alpha_c \sim 20$ the system diverges. The dynamical system behaviour shows stable limit cycles in the range $20 < \alpha < 30$. Therefore α, in the context of dynamical systems, can be considered as a bifurcation parameter. Stable limit cycles were obtained for $tU_m/D = 3500$ time steps which corresponds to 900 vortex shedding periods, based on frequency observed on the high velocity side. A time history of the critical limit cycle, $\alpha \simeq 20$, is shown Fig. 13.

A spectral density analysis of the dynamical system signals exhibits two main frequencies whose peaks are dominant for all modes under consideration. One frequency, at 155 Hz, appears to be consistent with the one drawn from the integral length scale analysis at $z/D = 0$. The second frequency, at about twice this value (316 Hz), is related to the frequency ($f_{pa} \sim 300$ Hz) of the mixing layer.

Furthermore, visualization of the reconstructed fluctuating velocity field (Eq. (3)), highlights a pulsed injection of fluid towards high velocity side at ~150 Hz (Braud, 2003) which is consistent with previous results.

4. Conclusions

The behaviours of mixing layers subjected to strong perturbations have been experimentally analyzed. These two configurations correspond to perturbations of the same nature, namely interactions with a wake. The first one concerns the modification of the initial conditions of the mixing layer when the second one corresponds to a perturbation occurring in the self-similar region of the flow, with a three-dimensional feature added by the cross-position of the wake.

The two approaches are also complementary owing to the fact that they use two experimental methods for solving the POD problem: the first one (hot wire anemometry) is well resolved in time but poorly resolved in space whereas the second one (PIV) is not able to reproduce time evolutions but is well resolved in space. Then, these two experiments contain different and complementary information on the large scale behaviour of perturbed mixing layers.

In the first configuration, two kind of mixing layers have been investigated: a *conventional* configuration utilizing a splitter plate with a bevelled trailing edge and a *thick* mixing layer utilizing a splitter plate with blunt trailing edge which resulted in the interaction of a mixing layer and a wake. The conventional configuration constitutes a reference case to analyze the effect of the dividing plate on the development of the shear layer. The results of this study confirm previous findings on the same kind of flow, namely the wake effect produced by the blunt trailing edge modifies the large scale organization. Its influence leads to a streamwise evolution of the flow in which two regions appear: a near wake region clearly dominated by the wake behaviour and a further downstream region in which the mixing layer overcomes the decreasing wake effect. The POD analysis of the flow field shows that longitudinal evolution strongly affects the large scale structures. The first two POD modes which are representative of the most energetic structures in the flow undergo a change in shape with the longitudinal distance from the trailing edge. As regards to the spatial POD modes, the transition between the region under influence of the wake and the "pure" mixing layer region is indicated by an inversion in the shape of the two first modes, the typical Gaussian-like shape of a classic mixing layer passing from the second to the first mode. In this region, the ratio of the first two eigenvalues λ_1/λ_2 is minimum and about 1.2. Hence, the flow is not strongly dominated by only one mode in this specific region. Moreover, when a spectral representation of the modes is considered, the first modes and their eigenvalues exhibit, in the near region, a frequency peak characteristic of the vortex shedding which occurs behind the dividing plate. This frequency corresponds to a Strouhal number based on the trailing edge thickness about 0.24. Downstream, this characteristic frequency progressively disappears as the wake influence is overcome by the mixing layer. Thus, the near wake region plays the role of a strong harmonic excitator of the shear layer as indicated by the modification of the flow organization and of the turbulent characteristics.

The second configuration concerns the interaction between a turbulent mixing layer and the wake of a cylinder perpendicular to it. It was first analyzed through the mean velocity-field which revealed a decomposition of the flow into distinct regions. It appears that the local injection of fluid from the low to the high velocity side just downstream of the cylinder is an important feature of the flow. The analysis of two point correlations in specific areas provided evidence of characteristic length scales and frequencies for the different regions depending on whether the flow was dominated by the mixing layer, the wake, or their interaction. These results were consistent with previous studies which showed an oblique vortex shedding in the wake when under the influence of the mixing layer. Slice POD was applied in the symmetry plane of the wake, $z/D = 0$. Eigenvalues and eigenvectors were calculated and it was found that it was possible to keep only the 15 first POD modes to construct a dynamical system accounting for the main characteristics of the flow. The LODS showed the same spectral characteristics as the experiments, namely the appearance of two dominant frequencies. The fluctuating velocities reconstructed from the dynamical system clearly showed a periodic fluid injection from the low to the high speed regions of the flow with a frequency and direction consistent with previous experimental observations.

Acknowledgements

This work has been partly supported by ONERA under Grant F/10.470/DA-RRAG and by the French Région Poitou-Charentes. L.P. acknowledges the financial support of the French Ministry of Defense (P. Moschetti). Authors also acknowledge fruitful discussions with Dr. J.J. Allen.

Appendix A

Equations leading to (8) are described in this section. Coefficients appearing in (7) are in the general 3D three components case:

$$\alpha_{nm} = \int_{\mathscr{D}} \mathbf{\Psi}^{(n)}(\boldsymbol{X})\mathbf{\Psi}^{(m)}(\boldsymbol{X})\,\mathrm{d}\boldsymbol{X} \tag{A.1}$$

- *First linear coefficient* $\boldsymbol{L}$*:*

$$L_{nm} = [\alpha_{nm}]^{-1}\int_{\mathscr{D}} \mathbf{\Psi}^{(n)}\Big[\vec{\mathrm{grad}}(\bar{\boldsymbol{u}})\mathbf{\Psi}^{(\mathrm{m})} - \vec{\mathrm{grad}}(\mathbf{\Psi}^{(\mathrm{m})})(\bar{\boldsymbol{u}}) - \vec{\mathrm{grad}}(\overline{\mathbf{\Omega}})\mathbf{\Phi}^{(\mathrm{m})} + \vec{\mathrm{grad}}(\mathbf{\Phi}^{(\mathrm{m})})\overline{\mathbf{\Omega}}\Big]\,\mathrm{d}\boldsymbol{X} \tag{A.2}$$

- *Second linear coefficient* $\boldsymbol{L}'$*:*

$$L'_{nm} = [\alpha_{nm}]^{-1}\int_{\mathscr{D}} \mathbf{\Psi}^{(n)}\Delta\mathbf{\Phi}^{(m)}\,\mathrm{d}\boldsymbol{X} \tag{A.3}$$

- *Quadratic coefficient* $\boldsymbol{Q}$*:*

$$Q_{nmk} = [\alpha_{nm}]^{-1}\int_{\mathscr{D}} \mathbf{\Psi}^{(n)}\Big(-\vec{\mathrm{grad}}(\mathbf{\Psi}^{(\mathrm{m})})\mathbf{\Phi}^{(\mathrm{k})} + \vec{\mathrm{grad}}(\mathbf{\Phi}^{(\mathrm{k})})\mathbf{\Psi}^{(\mathrm{m})}\Big)\,\mathrm{d}\boldsymbol{X} \tag{A.4}$$

Applied to the symmetry plane $z = 0$, and by considering only the symmetrical mode, these equations can be written:

$$\alpha_{nm} = \int_{\mathscr{D}} \left(\frac{\partial\phi_v^{(n)}}{\partial x} - \frac{\partial\phi_u^{(n)}}{\partial y}\right)\left(\frac{\partial\phi_v^{(m)}}{\partial x} - \frac{\partial\phi_u^{(m)}}{\partial y}\right)\mathrm{d}\boldsymbol{X} \tag{A.5}$$

- *First linear coefficient* $\boldsymbol{L}$*:*

$$L_{nm} = [\alpha_{nm}]^{-1}\int_{\mathscr{D}} \left[\frac{\partial\bar{w}}{\partial z}\left(\frac{\partial\phi_v^{(m)}}{\partial x} - \frac{\partial\phi_u^{(m)}}{\partial y}\right) - \bar{u}\left(\frac{\partial^2\phi_v^{(m)}}{\partial x^2} - \frac{\partial^2\phi_u^{(m)}}{\partial x\partial y}\right) - \bar{v}\left(\frac{\partial^2\phi_v^{(m)}}{\partial x\partial y} - \frac{\partial^2\phi_u^{(m)}}{\partial y^2}\right) - \frac{\partial\overline{\Omega}_z}{\partial x}\phi_u^{(m)} - \frac{\partial\overline{\Omega}_z}{\partial y}\phi_v^{(m)} - \left(\frac{\partial\phi_u^{(m)}}{\partial x} + \frac{\partial\phi_v^{(m)}}{\partial y}\right)\overline{\Omega}_z\right] \times \left(\frac{\partial\phi_v^{(n)}}{\partial x} - \frac{\partial\phi_u^{(n)}}{\partial y}\right)\mathrm{d}\boldsymbol{X} \tag{A.6}$$

- *Second linear coefficient* $\boldsymbol{L}'$*:*

$$L'_{nm} = [\alpha_{nm}]^{-1}\int_{\mathscr{D}} \left[\frac{\partial^3\phi_v^{(m)}}{\partial x\partial z^2} + \frac{\partial^3\phi_v^{(m)}}{\partial x^3} - \frac{\partial^3\phi_u^{(m)}}{\partial x^2\partial y} + \frac{\partial^3\phi_v^{(m)}}{\partial x\partial y^2} - \frac{\partial^3\phi_u^{(m)}}{\partial y^3} - \frac{\partial^3\phi_u^{(m)}}{\partial y\partial z^2}\right] \times \left(\frac{\partial\phi_v^{(n)}}{\partial x} - \frac{\partial\phi_u^{(n)}}{\partial y}\right)\mathrm{d}\boldsymbol{X} \tag{A.7}$$

- *Quadratic coefficient* $\boldsymbol{Q}$*:*

$$Q_{nmk} = [\alpha_{nm}]^{-1}\int_{\mathscr{D}} \left[-\phi_u^{(k)}\frac{\partial^2\phi_v^{(m)}}{\partial x^2} - \phi_v^{(k)}\left(\frac{\partial^2\phi_v^{(m)}}{\partial x\partial y} - \frac{\partial^2\phi_u^{(m)}}{\partial y^2}\right) + \frac{\partial\phi_w^{(k)}}{\partial z}\left(\frac{\partial\phi_v^{(m)}}{\partial x} - \frac{\partial\phi_u^{(m)}}{\partial y}\right)\right] \times \left(\frac{\partial\phi_v^{(n)}}{\partial x} - \frac{\partial\phi_u^{(n)}}{\partial y}\right)\mathrm{d}\boldsymbol{X} \tag{A.8}$$

References

Alfonsi, G., Restano, C., Primavera, L., 2003. Coherent structures of the flow around a surface-mounted cubic obstacle in turbulent channel flow. J. Wind Eng. Ind. Aerodyn. 91, 495–511.

Antonia, R.A., 1981. Conditionnal sampling in turbulence measurement. Annu. Rev. Fluid Mech. 13, 131–156.

Aubry, N., Holmes, P., Lumley, J., Stone, E., 1988. The dynamics of coherent structures in the wall region of a turbulent boundary layer. J. Fluid Mech. 192, 115–173.

Aubry, N., Guyonnet, R., Lima, R., 1991. Spatio-temporal analysis of complex signals: theory and applications. J. Stat. Phys. 64 (3/4), 683–739.

Bendat, J.F., Piersol, A.G., 1986. Random Data, second ed. Wiley and Sons, New York.

Berkooz, G., Holmes, P., Lumley, J.L., 1993. The proper orthogonal decomposition in the analysis of turbulent flows. Annu. Rev. Fluid Mech. 25, 539–575.

Bernero, S., Fiedler, H.E., 2000. Application of particule image velocymetry and proper orthogonal decomposition to the study of a jet in a counterflow. Exp. Fluids 29 (7), S274–S281.

Boldman, D.R., Brinich, P.F., Goldstein, M.E., 1976. Vortex shedding from a blunt trailing edge with equal and unequal external mean velocities. J. Fluid Mech. 75, 721–735.

Braud, C., 2003. Étude de la dynamique d'un écoulement à cisaillements croisés: interaction couche de mélange—sillage. Ph.D. thesis. Poitiers University, France.

Braud, C., Heitz, D., Braud, P., Arroyo, G., Delville, J., 2002. Investigation of plane mixing layer–wake interaction by means of two 2D PIV planes and of POD. In: International Symposium on Applications of Laser Techniques to Fluid Mechanics, 11th Session 32, Lisboa, Portugal.

Delville, J., 1995. La décomposition orthogonale aux valeurs propres et l'analyse de l'organisation tridimensionnelle des écoulements turbulents cisaillés libres. Ph.D. thesis Poitiers University, France.

Delville, J., Ukeiley, L., Cordier, L., Bonnet, J., Glauser, M., 1999. Examination of large-scale structures in a turbulent plane mixing layer. Part 1. Proper orthogonal decomposition. J. Fluid Mech. 391, 91–122.

Dziomba, B., Fiedler, H., 1985. Effect of initial conditions on two-dimensionnal free shear layer. J. Fluid Mech. 152, 419–442.

Heitz, D., 1999. Etude expérimental du sillage d'un barreau cylindrique se développant dans une couche de mélange plane turbulente. Ph.D. thesis. Université de Poitiers, France.

Holmes, P., Lumley, J., Berkooz, G., 1996. Turbulence, Coherent Structures, Dynamical Systems and Symmetry. Cambridge University Press.

Holmes, P., Lumley, J., Berkooz, G., Mattingly, J., Wittenberg, R., 1997. Low dimensional models of coherent structures in turbulence. Phys. Rep. 287, 337–384.

Johansson, P.B.V., 2002. The axisymmetric turbulent wake. Ph.D. thesis. Chalmers University of Technology, Gothenburg, Sweden.

Johansson, P.B.V., George, W.K., Woodward, S.H., 2002. Proper orthogonal decomposition of an axisymmetric turbulent wake behind a disk. Phys. Fluids 14, 2508–2514.

Koch, W., 1985. Local instabilities characteristics and frequency determination of self-excited wake flows. J. Sound Vib. 99, 53–83.

Lamballais, E., Silvestrini, J., 2002. Direct numerical simulation of interactions between a mixing layer and a wake around a cylinder. J. Turb. 3, 1–21.

Lumley, J., 1967. The structure of inhomogeneous turbulent flows. In: Yaglom, A., Tatarski, V. (Eds.), Atmospheric Turbulence and Radio Wave Propagation, pp. 166–178.

Ma, X., Karniadakis, G., 2002. A low-dimensional model for simulating three-dimensional cylinder flow. J. Fluid Mech. 458, 181–190.

Manhart, M., 1998. Vortex shedding from a hemisphere in a turbulent boundary layer. Theor. Comput. Fluid Dyn. 12, 1–28.

Metha, R.D., 1991. Effect of velocity ratio on plane mixing layer development: influence of the splitter plate wake. Exp. Fluids 10, 194–204, 1–28.

Michalke, A., Schade, H., 1963. Zur Stabilitat von freien Grenzschichten. Ing. Arch. 33, 1.

Ruelle, D., Takens, F., 1971. On the nature of turbulence. Commun. Math. Phys. 82, 137.

Stephen, A.V., Moroz, I.M., Read, P.L., 1999. POD analysis of baroclinic wave flows in the thermally-driven, rotating annulus experiment. Phys. Chem. Earth (B) 24 (5), 449–453.

Ukeiley, L., Cordier, L., Manceau, R., Delville, J., Bonnet, J.P., 2001. Examination of large-scale structure in turbulent plane mixing layer. Part 2. Dynamical systems model. J. Fluid Mech. 441, 67–108.